ORIGINAL ARTICLE

Fuzzy Parameters Integrated Markov Random Field (MRF) Model for Super Resolution Mapping (SRM) Over Vague Land Cover Regions

Welikanna, D. R. [*a] ⦿, Tamura, M. [b]

[a] *Department of Surveying and Geodesy, Faculty of Geomatics, Sabaragamuwa University of Sri Lanka, Sri Lanka*

[b] *Department of Civil and Earth Resources Engineering, Kyoto University, 615-8540 Kyoto, Japan*

ARTICLE INFO

ABSTRACT

The main objective of this study is to improve the Markov Random Field (MRF) based Super Resolution land cover Mapping (SRM) technique to optimize it performance for vague land cover classes. Additionally, the method could be used in order to minimize the point spread function (PSF) effects in multispectral data. In this regard, the study proposes a fuzzy class parameter estimated MRF model for the SRM generation. The paper describes two approaches for the pixel membership determination: spectral angle (SA) of each pixel and the fuzzy c-means (FCM) algorithm. Fuzzy class mean and the covariance measurements were derived using these memberships to model the class distributions within the MRF model. The use of fuzzy memberships can improve the overall posterior energy functions to reach a minimum, by taking both contextual and likelihood estimations of the V-I-S classes. The technique was tested using a WORLDVIEW-2 satellite image, acquired over a semi urban area in Colombo, Sri Lanka. Based on Visual interpretation three major land-cover types; vegetation, soil and exposed grass, and impervious surface (V-I-S) with low medium and high albedo were selected for the study. The bench mark reference data was generated using Maximum Likelihood Classification (MLC) performed on the same data resampled to 1 m resolution. The scale factor was set to be (S) =2, to generate SRM of 1 m resolution. The smoothening parameter (λ) which balances the prior and likelihood energy terms were tested in the range from 0.3 to 0.9. Fuzzy and conventional SRM were generated separately for each method. Both the methods produce satisfactory results with respect to its conventional counterpart with their own advantageous. Finally, the comparison of the model with the two non-parametric approaches: Support Vector Machine (SVM) and Neural Network (NN) are reported.

1 Introduction

Urban landscapes do not necessarily form a precise relationship between the actual pattern and the class label. The rapid change of the urban land cover categories within a small region, majority of land cover types being internally heterogeneous and intermediate conditions of the class boundaries make the urban landscape a vague entity (Forster, 1983; Wang, 1990; Wood and Foody, 1993). This situation on the ground leads to the formation of mixed spectral signature within a pixel of a satellite image (Duggin and Robinove ,1990; Zhang and Foody, 2001). Though the classes are mutually exclusive and discrete in the ground, it might not be the case in the image due to the sensor spatial resolution. Hence the pixel resolution plays a vital part in the interpretation process as it determines the amount of the mixed land cover components recoded within (Zhang and Foody, 2001). In many cases this brings fuzziness or the uncertainty into the image in the form of mixed pixels (Bastin et al., 2002; Fisher, 2010; Fisher et al., 2006). The conventional classification methods force these mixed pixels to get classified into a single class. Owing to these complications, many previous studies have highlighted the importance of dealing a pixel as a mixed element (Fisher, 1997; Foody ,1997). Fuzzy set theories have been used extensively to address this imprecise class information in a mixel (pixel comprising mixed land cover categories) (Maselli et al., 1995; Zadeh, 1965). Although it

---

should be noted that fuzzy parameter integrated classification schemes do not fully resolve the problem of class mixtures within the pixel, it provide more appropriate definition for vague land cover classes recorded at a particular sensor resolution (Fisher and Pathirana, 1990). In many classification schemes defining an accurate relationship between the features in the feature space and the class labels is very important (Tso and Mather, 2009). When this relationship takes the form of one-to-many, a fuzzy classification output can be expected. The heavy spectral and spatial overlap of the land cover classes also adds difficulties to their interpretation. Hence it is important to consider both the spectral and spatial dependencies to correctly classify a pixel. MRF have been potentially identified in Remote Sensing image classification with promising results, mainly due to its ability to integrate the contextual based information in to the classification scheme (Kasetkasem et al., 2005; Solberg et al., 1996). This practical applicability of MRF has been made possible by the equivalence between MRF and Gibbs distribution, established by the Hammersley-Clifford theorem (Li, 2009; Tso and Mather, 2009). This provides a convenient framework to determine the joint prior probability for the pixel labelling problem.

One of the main applications of the MRF is to produce higher resolution land-cover maps, also called SRM, from coarser resolution satellite images (Kasetkasem et al., 2005; Welikanna et al., 2008). Moreover MRF models have been widely used to resolve many of the vision problems including image restoration and segmentation, edge detection, texture analysis, data-fusion and change detection (Ardila et al., 2011; Dubes et al., 1990; Kasetkasem and Varshney, 2002; Xu et al., 2011). Many of this work resulted in improving the technique. Furthermore this has led to a deeper understanding of its performance and parameter estimation. MRF based SRM technique was developed using class descriptive statistics in the form of conventional class mean and covariance to model their probability density functions. The conventional mean and covariance consider a training pixel to belong to a single class (one pixel one class) while neglecting its proportional contribution. Several previous studies have integrated fuzzy class parameters into a classification scheme. In contrast to conventional methods, a fuzzy supervised classification method using fuzzy mean and the fuzzy covariance showing the determination of pixels relation to a land cover class by the means of membership grades, enables more accurate statistical parameter determination for the classification scheme (Wang, 1990). The importance of identifying the mixel and using the membership grades to utilize more of its spectral information in the classification scheme is highlighted in this study. In another effort, fully-fuzzy supervised classifications with statistical (modified fuzzy C-mean clustering algorithm) and neural network based classifiers have been tested with improved classification results(Zhang and Foody, 2001). Indicator Kriging based interpolation was implemented in this study to estimate the class membership grades for the training pixels. Fuzzy parameter integrated Spectral Mixture Analysis (SMA) classification technique was also tested in another study

consistently (Tang et al., 2007). It went on to show the improvement achieved in the classification with respect to the MLC, linear SMA and partial fuzzy methods. In this study we propose a robust MRF model which integrates the fuzzy class descriptive statistics defined by using SA and FCM techniques. The results were compared with respect to MLC, SVM and NN based results as the leading parametric and non-parametric classification techniques.

2 MRF and Fuzzy parameter estimation for remote sensing images

MRF can be considered as the most popular undirected graphical models in vision which provide the feasibility to integrate the contextual information to a labelling problem. In any real image, adjacent pixels are correlated due to the point spread function (PSF) effect and the distribution of ground cover types over regions lager than that of the spatial resolution of the image (Richards and Jia, 2006). Therefore with the use of the contextual information, pixels will no longer be treated as an isolated entity. MRF with its relationship to the Gibbs Random Fields (GRF), establish the framework to model the joint distribution of labels and data. A comprehensive introduction to this can be found in the literature (Li, 2009; Tso and Mather, 2009). This section is dedicated to describe the formulation an image classification model with in a MRF frame work.

Let a set of pixel DN values in an observed image $\mathbf{x}$ with K spectral bands, to be represented by $x_1 \dots x_m$, where M is the total number of pixels to be classified. The measurement vectors are represented as $x_m, m = 1, \dots M$ in a pixel matrix $A \in (M_1 \times M_2)$ where M_1 and M_2 are the dimensions of the matrix. Let $\mathbf{c}$ be the resulting SRM defined on a pixels matrix B, with each of the pixel belonging to a unique class at a finer resolution than the observed image. Let an unobserved multispectral image be $\mathbf{y}$ with the same number of spectral bands as $\mathbf{x}$ but with a spatial resolution identical to $\mathbf{c}$. The pixel location in y is represented by $y_{i,j}$. Also it is assumed that each pixel in y can be assigned to a unique class $c(y_{i,j})$. If the pixel resolution of the original image is R and that of the SRM is r $(<R)$, the relation between the two images is determined by a scale factor which is denoted by $S=R/r$. Hence it can be seen that the pixel matrix $B = SM_1 \times SM_2$. In this study S is set to take an integer value for convenience. For each pixel $y_{i,j}$ a symmetric neighbourhood $N(y_{i,j})$ is defined by a window size W, where it is the length of the side of the squared window. Different definitions for the neighbourhood system can be found in the literature (Li, 2009). A second order neighbourhood consisting the eight closest connected pixels (*W=3*) have been selected for this study. The classified image $\mathbf{c}$ will be modelled as a MRF with respect to the neighbourhood system $N(y_{i,j})$. MRF is defined by local properties, therefore the labelling of the pixels is considered to be effected by this neighbourhood configuration (Tso and Mather, 2009). It is here the MRF models take the advantage of modelling contextual dependencies, or the spatial correlation among the pixels. The set ω is referred as a random field with the probability

distribution p(ω) describing the likelihood of finding the labels $c(y_{i,j}) = \omega \in \{1, .. l\}$ over the image for l number of land cover classes. The overall objective of the model is to classify all the pixels which maximize the global posterior probability p(ω|**x**), which is the probability that ω is the correct overall scene labelling given the full set of measurement vectors **x**. According to the Bayes theorem, a pixel x_m in the observed image is allocated to a class ω according to equation (1), where a value ω is selected to maximize the argument for a pixel to find the most appropriate scene label $\overline{\omega}$.

$$\overline{\omega} = argmax\{p(\mathbf{x}|\omega)p(\omega)\} \tag{1}$$

According to the equivalence of the MRF and the GRF, the probabilities can be modelled as energy functions. Hammersley-Clifford theorem explains the existence of a unique GRF for every MRF as long as the GRF is defined by the cliques on a neighbourhood system. A clique is a subset in which all pairs of the pixels are mutual neighbours (Tso and Mather, 2009). Hence the prior probability p(ω) for the SRM, the conditional probability p(**x**|ω), that the image **x** is observed given the true SRM and the posterior probability p(ω|**x**) are modelled by means of energy functions.

$$P(\omega|\mathbf{x}) = \frac{1}{Z}\exp(-U(\omega|\mathbf{x})/T) \tag{2}$$

Where Z is the normalizing constant, T is the constant termed temperature and U(ω|**x**), is the posterior energy function of the super resolution map **c** given the observed image **x** . Both the terms Z and T are independent of ω and **x**. Based on equation (2), it is clear that maximizing the probability p(ω|**x**) is equivalent to minimizing the energy function U(ω|**x**).

2.1   Prior Energy for contextual dependencies

In the MRF, prior and likelihood energies are modelled individually. They account for the contextual and spectral properties of the observed image respectively. The prior energy is modelled by using the sum of pair-site interaction within the neighbourhood system $N(y_{i,j})$ as follows:

$$U(\omega) = \sum_{i,j} U\left(c(y_{i,j})\right) = \sum_{i,j}\sum_{i\in N(y_{i,j})}\beta[1 - \delta(c(y_{i,j}), c(y_l)) \tag{3}$$

The term $\delta(c(y_{i,j}), c(y_l)$ is called the "Kroneker delta", which takes a unit value when $\delta(c(y_{i,j})) = c(y_l)$ and 0 otherwise (Richards and Jia, 2006). $\beta > 0$ controls the influence of the neighbouring pixels, and can be an anisotropic or isotropic assumption made by the user. In this study this value is an isotropic expression which only depends on the Euclidian Distance D between the pixels $y_{i,j}$ and y_l, is calculated by $\frac{1}{\omega}[D(c(y_{i,j}, y_l))]^{-2}$, where $\overline{\omega} = \sum_{i\in N_{i,j}} D(c(y_{i,j}, y_l) = 1$ is the normalizing constant. In equation (3), each pixel contributes locally to the prior energy, which is denoted as $u(c(y_{i,j}))$. A single pixel in the

observed image is assumed to follow a multidimensional normal distribution, which is determined by the mean and the variance of each spectral class. These fundamental parameters have been reformed using fuzzy definitions to determine the likelihood energy in the MRF.

2.2   Determination of Fuzzy parameters through SA and fuzzy C mean clustering

Fuzzy set theory (Zadeh, 1965) provides the conceptual framework to solve the classification problems in an ambiguous environment. In the problem of image classification, if we take an event ω which is a class label and consider it to be a fuzzy subset of the universe of discourse ψ, and **x** to be a feature vector of a particular pixel, then the probability density function (PDF) of ω can be represented by a fuzzy membership function f_ω as follows

$$p(\omega) = \int_\psi f_\omega(x_i) \tag{4}$$

This multiple membership values for a feature vector realize to what extent it belongs to a land cover class label; and redefine its contribution to the class mean and the variance. This is a more feasible approach to model the geometrical shapes of different clusters within the same data set. Accordingly, the discrete fuzzy mean and the fuzzy covariance matrices can be derived from the definitions given by Wang (1990). Essentially this approach restructures the conventional mean and the covariance using fuzzy membership function. Two different techniques were tested to define the fuzzy membership for each training pixel. In the first case, we introduce the spectral angle of each pixel to be used as the pixel membership. While in the second method, fuzzy c-mean clustering is used. The spectral angle is used to unmix the pixel to classes of interest If $f_\omega(x_i)$ is the fuzzy membership value for the pixel vector $x_i \equiv x_m$ in the observed image **x,** the membership value was determined by calculating the spectral angle in radiance between the training pixel vector (x_i) and the reference spectra of the classes (r_i) as shown below.

$$f_\omega(x_i) = cos^{-1}\left[\frac{\sum_{i=1}^K x_i r_i}{\sqrt{\sum_{i=1}^K x_i^2 \sum_{i=1}^K r_i^2}}\right] \tag{5}$$

The FCM approach clusters the data with fuzzy means and the fuzzy boundaries. It provides a relationship between the pixels and the classes using a fuzzy c partition. The image **x** (when K=1) is portioned into a n × c matrix (F) with each element of the matrix $(f_\omega(x_i))$ showing the pixel membership value for class ω. The J function measures the difference between each pixel values and the cluster centres μ to estimate the U matrix (Mather 2009). The clustering criterion can be shown by the following equation.

$$J_w(F,V) = \sum_{i=1}^{n} \sum_{\omega=1}^{c} (f_\omega(x_i) \times (x_i - \mu_\omega)^2) \tag{6}$$

Where $V = (\mu_1, \mu_2, \dots \mu_c)$ is the vector of the cluster canters, and w being the membership weighting exponent $1 < w < \infty$. A local minimum for J_w can be achived under the condition shown in equation (7). Hear $w > 1$ and $x_i \neq \mu_\omega$. In an instance of K spectral bands the average values of the memberships in each band gives the best estimation.

$$f_\omega(x_i) = \frac{1}{\sum_{j=1}^{c} \left[\frac{|x_i - \mu_\omega|}{|x_i - \mu_j|} \right]^{\frac{2}{(m-1)}}} \tag{7}$$

In the case of per-class covariance matrices, let the training pixels take values $x_1, x_2 \dots x_n$ with n being number of training pixels for l number of classes. Then the respective fuzzy training data set can be represented as a fuzzy set $\{F_{l \times n}/f_{i,j} \in [0.0, 1.0]$. The element $f_{i,j}$ represents the fuzzy membership value of a training pixel $x_j (1 \leq j \leq n)$ to the class l. The discrete fuzzy mean $\overline{\mu_\omega}$ and the fuzzy covariance matrix $\overline{\sum_\omega}$ for class ω can be defined as follows:

$$\overline{\mu_\omega} = \frac{\sum_{i=1}^{n} f_\omega(x_i) x_i}{\sum_{i=1}^{n} f_\omega(x_i)} \tag{8}$$

$$\overline{\sum_\omega} = \frac{\sum_{i=1}^{n} f_\omega(x_i)(x_i - \overline{\mu_\omega})(x_i - \overline{\mu_\omega})^T}{\sum_{i=1}^{n} f_\omega(x_i)} \tag{9}$$

Parameters were estimated using the coarser resolution image. To determine the class membership grades for each pixel, different approaches can be found in the literature, and for an evaluation among these approaches additional research is required. In this study, the use of SA and FCM approaches provide us the means to investigate any bias in the model to a specific membership grade definition. A single pixel in the coarser resolution image **x**, corresponds to s^2 pixels in the finer resolution SRM, **c**. Hence the PDF of an observed pixel vector x_m is assumed to be normally distributed with respect to the pixel composition with mean $\overline{\mu(x)}$ and covariance $\overline{\sum(x)}$, which can be defined using equations (10) and (11) as follows:

$$\overline{\mu(x)} = \sum_{\omega=1}^{l} \theta_\omega(x) \overline{\mu_\omega} \tag{10}$$

$$\overline{\sum(x)} = \sum_{\omega=1}^{l} \theta_\omega(x) \overline{\sum(x)} \tag{11}$$

Here θ_ω is the proportion of the class ω in a pixel x_m, where $\sum_{\omega=1}^{L} \theta_\omega(\mathbf{x}) = 1$. We also assume the spectral values of s^2 fine resolution pixels $y_{i,j}$ are independent and identically distributed, according to the normal distribution of the parameters of class $c(y_{i,j})$.

2.3 Fuzzy likelihood Energy generation

The conditional distribution of the observed data **x** with the given true class labels ω, is assumed to be Gaussian. We also assume a coarser spatial resolution pixel of the original image to contain a number of pure pixels at the fine spatial resolution. These fine spatial resolution pixels are strictly assumed to be spatially un-correlated. Therefore, the fuzzy mean and the fuzzy covariance matrix of the observed pixel at a coarser resolution scale are directional sum of fuzzy mean vector and the fuzzy covariance matrix of the corresponding pixels at the fine resolution scale. Hence the conditional probability density function (PDF) in equation (1) for the observed image can be defined as follows:

$$p(\mathbf{x}|\omega) = \prod_m \frac{1}{(2\pi)^{k/2}|\overline{\sum(x)}|} \exp(-\frac{1}{2}(x_m - \overline{\mu(x)})^t \overline{\sum(x)}^{-1}(x_m - \overline{\mu(x)})) \tag{12}$$

The likelihood energy in this case with respect to the relationship shown in equation (2) takes the form written by:

$$U(\mathbf{x}|\omega) = \sum_{m,l} [(x_m - \overline{\mu(x)})^t \overline{\sum(x)}^{-1}(x_m - \overline{\mu(x)}) + \frac{1}{2}ln|\overline{\sum(x)}|] \tag{13}$$

The posterior energy function is established using the definitions of the Bayes theorem which combine the prior and the likelihood energy terms defined in equations (3) and (13) as follows:

$$U(\omega|\mathbf{x}) = U(\omega) + U(\mathbf{x}|\omega) \tag{14}$$

According to equation (2), the minimum of the posterior energy provides the optimum SRM $\omega \in C$, which is the maximum a posterior probability solution for the SRM problem (Geman and Geman, 1984). To control and balance the spectral and the contextual information flow during the SRM generation a parameter called "the smoothness parameter" $0 \leq \lambda < 1$ is introduced to the posterior energy function in equation (11). Hence the full form of the posterior energy function can be written as:

$$U(\omega|\mathbf{x})) = \lambda U(\omega) + (1 - \lambda)U(\mathbf{x}|\omega) \tag{15}$$

The MAP estimation of the posterior energy in equation (12) is determined by using the stochastic Simulated Annealing technique (SA). This implements a Metropolis-Hasting sampling technique to reduce the energy to yield the maximum a posterior solution. A comprehensive explanation about the SA technique can be found in literature (Li, 2009; Tso and Mather, 2009). Below figure (Fig. 1) details the major outlines of the proposed approach.
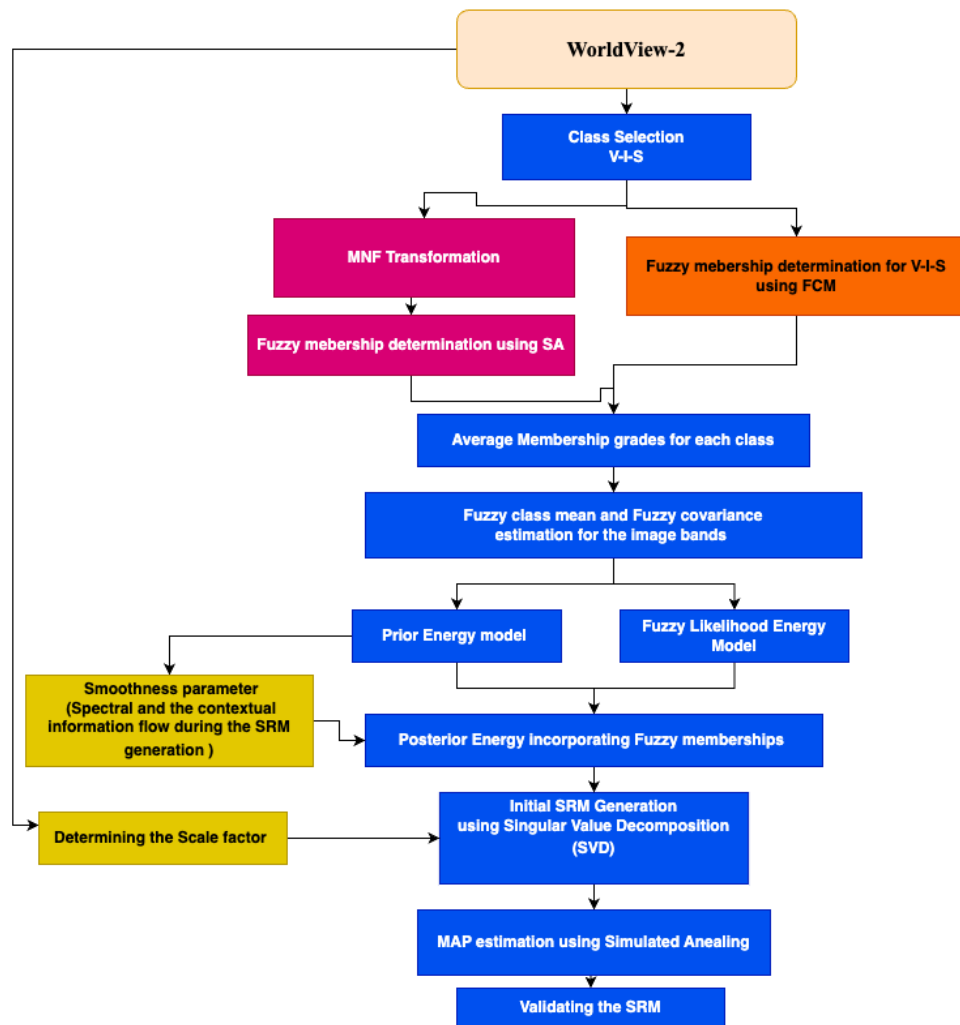
Fig. 1: The conceptual work flow for the development of Fuzzy MRF models.
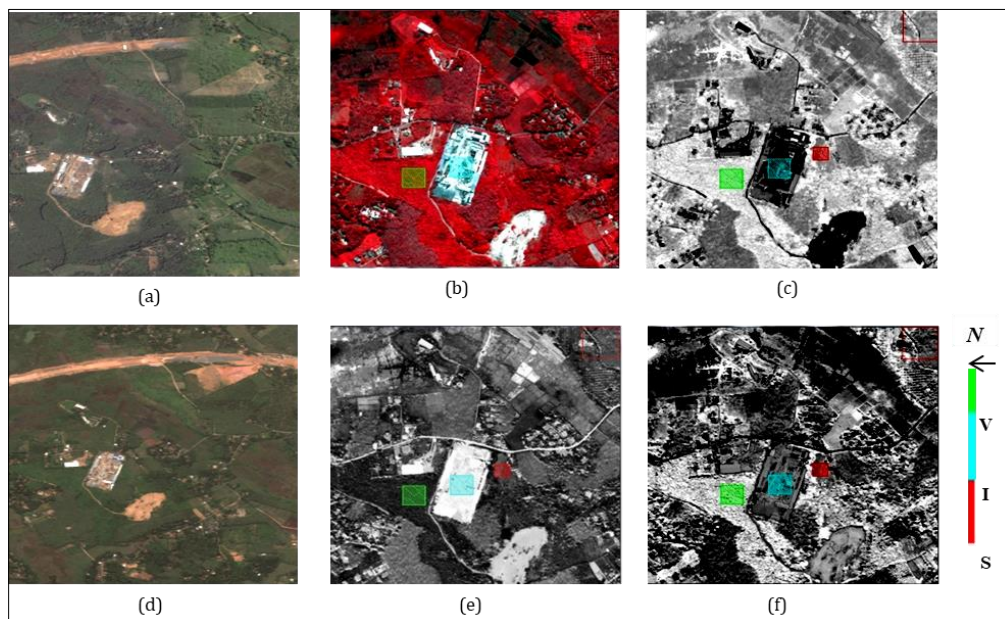

Fig. 2: Google map image of the study site in the west coast of Sri Lanka, (a) for year 2007 and (d) 2009, (b) the Worldview-II false colour multispectral band composite RGB (6, 5, 4) showing the selected ground samples, (c), (e) and (f) fractional images generated by SA, for V-I-S classes.

3   Study area and data processing

The fuzzy parameter integrated MRF based SRM technique was tested using real satellite images. The selected study area was in the southwest urban coastal zone of Sri Lanka. In particular this area is undergoing a major construction of a highway running from the south to north. Due to the heavy construction activities, the land cover of the region is exposed to considerable amount of change. The major land-use/land cover classes occurred in this region includes Vegetation, Impervious Surface ranging from low to high albedo, Exposed Soil and Grass and Water. Out of these major land cover classes, three main classes were considered for the study, Vegetation (V), Impervious surface (I) and exposed grass and Soil (S). This selection was influenced by the Ridd`s (Ridd, 1995) V-I-S model determining the urban composition. Considering the heterogeneity of the land-cover categories in this area, it is observed that the area is transforming towards a complete urban settlement. Fig. 2 provides the details of the study area, with the Google map images showing the land cover changes during the year 2007 to 2009.

An image subset from the DigitalGlobe's WorldView-2 satellite acquired on 29th January 2010 was employed in this study. Worldview-2 satellite provides additional coastal (400-450 nm), yellow (585-625 nm), red edge (705-745 nm) and Near-IR2 (860-1040 nm) bands at a spatial resolution of 1.84 m at nadir, and 2.08 m at 20° off-nadir in addition to the typical multispectral bands: Blue (450-510 nm), Green (510-580 nm), Red (630-690 nm) and Near-IR (770-895 nm) (DigitalGlobe, 2011). The image was preliminary processed to determine the membership grades for each training pixel using SA and fuzzy c-means clustering technique. In the case of SA, the Minimum Noise Fraction (MNF) transformation was employed to remove the correlation exists between the eight bands to identify the pure pixels. Different techniques for the selection of the pure pixels can be found in the literature but here we have employed a supervised end-member selection using the n-D spectral space. After generating the reference spectra using the spectral angle for each pixel, pixels were unmixed for corresponding land cover components (Krus et al., 1993). The Spectral Angle Mapper (SAM) technique employed here measures the spectral similarity between the end member pixel spectra and the original pixel spectra based on the angle between vectors of the two spectra's. The use of SAM in this study was encouraged due to several important reasons, SAM does not necessarily affect to illumination and the albedo effects, image has not been corrected for the atmospheric effects and higher class spectral sperability (Transform Divergence (TD) and Jeffries-Matusita distance (JM) being very close to 1.9 and 2.0 for the randomly test samples over the study area). The ability of the SAM to withstand different atmospheric and topographic variation is because that these effects linearly scale the spectra of the unclassified pixel vector and the vectors of the reference signatures belonging to same class, with least effect on the spectral angle (Sohn et al., 1999). The square homogeneous training samples chosen for the three classes to determine the fuzzy class parameters, and the fractional abundance for each of the V-I-S components are shown in the Fig. 2. These fractional estimations were then assigned as the training pixel membership values.

To simplify the calculation process, the training samples were selected to be square. For vegetation and the impervious surface, the total number of training pixels was 900 while for the soil class it was selected to be 400.

Table 1: The mean values for each class in different spectral bands using Fuzzy (SA), Fuzzy c-Means, and Conventional techniques.

Band		1	2	3	4	5	6	7	8
Vegetation	**Fuzzy (SA)**	362.99	274.47	355.50	242.71	79.46	553.95	510.57	715.65
	Fuzzy C-Mean	363.06	274.63	358.80	245.76	80.45	558.92	510.92	715.94
	Conventional	363.02	274.57	355.46	242.97	79.66	552.27	508.14	712.30
Impervious	**Fuzzy (SA)**	478.60	443.49	617.311	581.744	261.25	515.35	308.05	411.22
	Fuzzy C-Mean	472.41	430.27	581.64	533.93	236.64	473.91	285.74	380.71
	Conventional	476.98	441.38	614.40	579.49	260.42	516.58	310.50	415.67
Soil	**Fuzzy (SA)**	378.34	299.54	378.28	294.68	115.59	504.69	432.93	634.73
	Fuzzy C-Mean	378.41	299.72	378.50	294.94	115.82	503.07	431.04	632.64
	Conventional	378.33	299.36	377.15	293.87	115.28	499.10	426.93	625.40

Table 2: Covariance matrices for vegetation class (a) using SA, (b) using Fuzzy c-Means, and (c) Conventional case.

(a)

Band 1	2	3	4	5	6	7	8
8.95	8.89	27.79	26.85	11.31	66.99	50.90	74.05
8.89	17.78	51.48	45.43	21.88	102.98	81.81	113.53
27.79	51.48	327.33	239.69	75.85	846.04	715.93	919.13
26.85	45.43	239.69	228.09	77.90	629.70	446.45	644.17
11.31	21.88	75.85	77.90	39.69	136.06	83.01	125.50
66.99	102.98	846.04	629.70	136.06	3097.72	2706.23	3676.97
50.90	81.81	715.93	446.45	83.01	2706.23	2768.35	3470.08
74.05	113.53	919.13	644.17	125.50	3676.97	3470.08	4931.17

(b)

Band 1	2	3	4	5	6	7	8
9.45	10.07	27.31	29.47	13.40	64.95	51.30	76.66
10.07	19.26	52.03	51.19	25.42	107.99	84.31	127.13
27.31	52.03	344.90	254.76	79.32	921.17	793.28	1027.40
29.47	51.19	254.76	249.87	89.78	664.84	485.57	708.60
13.40	25.42	79.32	89.78	47.43	136.78	79.92	135.92
64.95	107.99	921.17	664.84	136.78	3414.33	3066.42	4118.57
51.30	84.31	793.28	485.57	79.92	3066.42	3165.75	3951.29
76.66	127.13	1027.40	708.60	135.92	4118.57	3951.29	5513.88

(c)

Band 1	2	3	4	5	6	7	8
8.70	8.27	26.74	25.00	10.01	68.29	53.52	77.40
8.27	16.24	48.40	41.31	19.03	103.05	84.82	117.26
26.74	48.40	319.02	229.69	69.67	838.48	714.50	917.25
25.00	41.31	229.69	212.68	69.04	625.45	452.71	652.42
10.01	19.03	69.67	69.04	33.93	135.33	88.72	132.51
68.29	103.05	838.48	625.45	135.33	3067.91	2683..14	3639.24
53.52	84.82	714.50	452.71	88.72	2683.14	2743.24	3432.85
77.40	117.26	917.25	652.42	132.51	3639.24	3432.85	4871.06

It should also be mentioned that with the membership values being determined for each training pixel, the required number of training pixels needed to define the class probability density should necessarily decrease. Initial parameter determination was performed at a 400×400 pixel image subset, while for the MRF based SRM input it was further reduced to a 100×100 pixel image to cut down the processing time.

In the second approach, a fuzzy c-means clustering membership matrix was generated for each pixel of the training samples in each band (Tso and Mather 2009). Then the average value of the 8 bands for a pixel is calculated for each class. These averaged membership values for each pixel is considered to be its final membership to that class. The statistical parameters mean and covariance, generated from the conventional and the fuzzy algorithms are different. Fuzzy means for the three classes (V-I-S) and the

fuzzy covariance matrices for the vegetation class generated from the Fuzzy (SA), Fuzzy c-Means, and Conventional techniques are shown in Table 1 and Table 2 respectively. It can be seen from these results that the inclusions of the fuzzy class parameters makes significant changes to the class probability density functions in a Gaussian framework.

The bench mark reference images were produced by performing the hard Maximum Likelihood classification (MLC), using the same training samples implemented for the class parameter estimations. As the generated SRM resolution is 1 m, prior to the MLC classification the images were resampled to 1 m resolution using a scale factor of 2, for the pixel to pixel cross comparison. Considering the distribution of the classes in the study region, to avoid the original pixels being over resampled, the nearest neighbour resampling technique has been employed. For the determination of the class composition within a pixel to generate the initial SRM maps, we used the Singular Value Decomposition (SVD) technique (Canty, 2010). In SVD, a library matrix determined by the class mean vector is inverted by decomposing it to two column orthogonal matrices and a diagonal matrix to perform a vector multiplication with the observed image to get the least square estimate of end member abundance (Boardman, 1989). If the fractional estimation for a particular class in a pixel $x_i \in A$ in the observed image is θ_i, then there will be $\theta_i \times S^2$ allocation of that class in the corresponding pixel set B of the SRM. The generated initial SRMs using the SVD fractions is shown in Fig. 3(b), and essentially, this initial configuration will be optimized with Conventional, SA and FCM based MRF scheme.

4   Experimental Results

To understand the effects of the fuzzy parameter integration a combination of SRM were generated using conventional, SA and FCM based class estimations for a range of smoothness parameters (λ). The results are shown in the Fig. 3. It is important to mention that the λ is a key parameter which controls the contribution of the prior and the likelihood energy in the posterior energy determination. For example when λ=1 the likelihood term is completely ignored in equation (15) for a minimal posterior energy, forcing all the pixels to be classified to a single class. The validation of the SRM at both pixel level as well as the sub pixel level is a complex process. This becomes even tricky when proper ground truth information is not available. But for performance evaluation among the techniques carefully selected identical ground samples can be kept constant to see the variability in the class PDF estimations. In this study we implement two approaches to validate the SRM results with the MLC results. In the pixel based validation, we used the Cohen`s kappa statistics (Congalton, 1991), which is also known as kappa coefficient to assess the accuracy of the generated SRM using the contingency tables. For the sub pixel based validation we used the mean absolute error

(MAE) (Tang et al., 2007) to compare the class area proportion within a fixed area size, between the SRM and the reference images. The MAE is defined as follows (Welikanna et al., 2021):

$$MAE_l = \frac{\sum_{m=1}^{N}\sum_{l=1}^{l}\left|SRM_{fr_l}(m)-Ref_{fr_l}(m)\right|}{N} \qquad (15)$$

Where N is the total number of pixels considered. The $SRM_{fr_l}(m)$ and $Ref_{fr_l}(m)$ are the fractional value of class l in a fixed area m of the SRM and the reference image respectively.

MAE provides an average measure of the agreement of the class fractions that has changed within a fixed area from the ground truth to thematic output. Hence a small error clearly leads to a better agreement between the two inputs. According to the previous experiments done on the parameters of the MRF technique it has been observed that for smaller scale factors $S \le 4$, λ takes the values in the range of 0.7 to 0.9 (Tolpekin and Stein, 2009) to genere the optimum SRM. Accordingly, in this study for S = 2, the highest accuracy of the SRM with respect to the reference image was attained at λ = 0.9, for fuzzy as well as for the ordinary MRF models.

Table 3: Kappa and OA agreement.

	λ	OA	Kappa
	0.9	77.70%	0.65
Conventional MRF	0.8	77.26%	0.64
	0.7	75.94%	0.62
	0.9	85.71%	0.78
SA parameter based MRF	0.8	84.52%	0.76
	0.7	83.04%	0.74
	0.9	85.57%	0.78
Fuzzy c-means parameter based MRF	0.8	85.25%	0.77
	0.7	83.93%	0.75

The Table 3 reveals the steady increase of the kappa agreement between reference and the SRM generated at λ = 0.7, 0.8, 0.9 for the three models. At λ = 0.9 the highest accuracy SRM is generated with a kappa agreement of 0.78 for both SA and FCM approaches while 0.65 in the conventional approach (Table 3). A visual inspection of the SRM in the Fig. 4 also justifies this result, with smoother SRM resulting in the fuzzy based approaches with respect to its conventional counterpart. For the total λ range investigated from 0.3 to 0.9 (Fig. 3) the FCM and SA models have produced SRM maps more close in
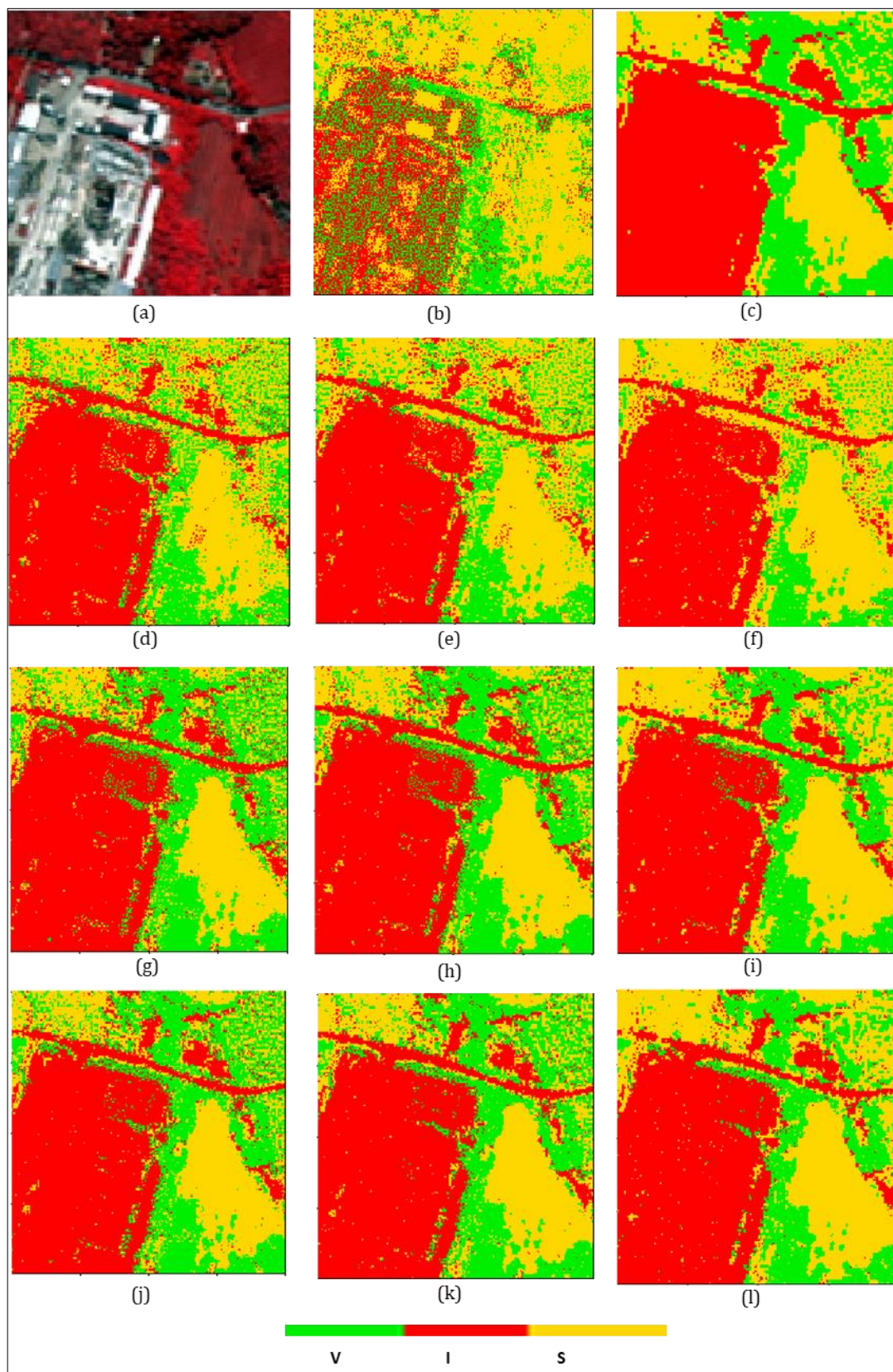
Fig. 3: (a)100×100 Worldview-II false colour multispectral band composite RGB (6, 5, 4), (b) Initial SRM, (c) MLC reference image, (d), (e), (f) optimum SRM generated at λ=0.7, 0.8, and 0.9 for the conventional case, (g), (h), (i) optimum SRM generated at λ=0.7, 0.8, and 0.9 using SA, and (j), (k), (l) optimum SRM generated at λ=0.7 ,0.8, and 0.9 using the fuzzy c-means class parameter estimations.

agreement with the MLC reference map with the kappa values ranging from 0.7 to 0.78, where in the conventional case it was at 0.55 to 0.65. This clearly suggest that the fuzzy class parameter estimation inside the MRF based SRM model has a significant influence in its performance.
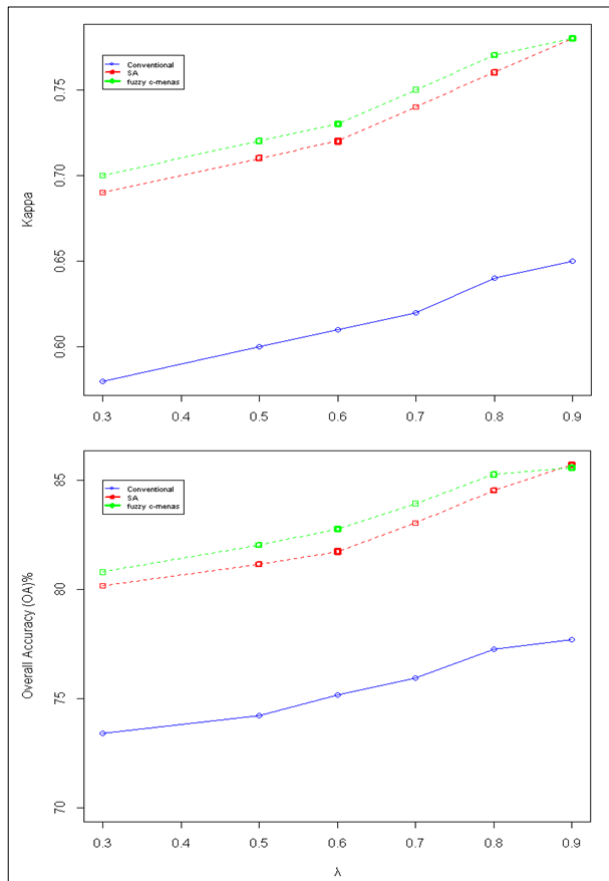

Fig. 4: Kappa and the Overall Accuracies for the Fuzzy and the Conventional MRF models for λ values ranging from 0.3 to 0.9.

Table 4 shows the error matrices generated for the fuzzy MRF model using SA and FCM approaches and the conventional SRM. From the table, the user accuracy (reliability) for the Grass and exposed soil class is 74% and 72% in the fuzzy MRF models using SA and FCM definitions respectively. But in the conventional case this was 58%. Grass and exposed soil class attains a comparatively higher degree of uncertainty in the parameterization than the other two classes in this study. This is mainly due to its higher mixture with the vegetation class. The joint distribution of normally distributed two variables is expected to be a Gaussian distribution. The determination of the class fractions are from normally distributed pixel vectors of the class samples. These fractions assigned as the membership grades tend to preserve the original distribution and provide better probabilistic measures for classes within a pixel. This affects the pixel labelling problem with the fuzzy MRF model, demanding the pixels to have accurate statistical measure through the prior and likelihood energy determination than in the conventional

method. Hence, with the use of the membership grades the classification results has significantly improved for the soil class. The persistence of the classification agreement between the ground truth classes and the thematic classes for the vegetation and impervious categories are slightly higher in the fuzzy parameterized MRF model than its conventional case. This can be seen from the diagonal elements of the error matrices.

The validation was carried out mainly to compare the fuzzy and the conventional MRF results for their performance at a pixel level. But it has certain draw backs as the error matrix doesn't provide the convenience to evaluate the effect of the multiple memberships' assignment for each pixel and also the fractional agreement of the fuzzy classification.

Table 4: Confusion Matrices.

SA Based MRF		Ground Truth Classes		
		Vegetation	Soil	Impervious
Thematic Classes	Vegetation	7346	870	565
	Soil	2296	9803	1129
	Impervious	406	495	17090

FCM based MRF		Ground Truth Classes		
		Vegetation	Soil	Impervious
Thematic Classes	Vegetation	7232	893	427
	Soil	2466	9856	1216
	Impervious	350	419	17141

Conventional MRF		Ground Truth Classes		
		Vegetation	Soil	Impervious
Thematic Classes	Vegetation	4403	733	101
	Soil	5193	9968	1932
	Impervious	452	467	16751

To evaluate the fractional agreement between the optimal SRM and the reference images, MAE error measure has also been employed. A fixed area size for the comparison was set to 5×5 pixel area. This fixed area size is chosen so that in this region, the MLC classified output provides the necessary mixture condition for all the three classes to have fractional estimations. The definition of the fixed area can vary depending on the heterogeneity of the classes in the study region. The proportions of the classes within this fixed area of 5×5 pixels were determined for both the SRM and the reference images.

The MAE for the fuzzy integrated MRF model and the conventional model based SRM are shown in Table 5. According to the table, the average MAE for both the SA and FCM based fuzzy MRF models are close to each other with a value of 0.03 and smaller with respect to the conventional

Table 5: MAE for the Fuzzy Integrated MRF models and the Conventional MRF model.

	SA parameter based MRF	Conventional MRF	Fuzzy c-Means based MRF
Vegetation	0.03	0.12	0.04
Soil	0.05	0.15	0.06
Impervious	0.02	0.03	0.02
Average MAE	0.03	0.10	0.03

case where it is 0.1. This is a useful result to further understand the healthier performance of the fuzzy parameter integrated schemes.

To further understand the performance of the proposed model with respect to different classification techniques, we cross validate the SRM results with SVM and NN based classifications. We chose a pixel based comparison using error matrices to compare these techniques. The choice of the two classification techniques SVM and NN were made mainly because of their ability to classify remote sensing images nearly as accurate as the statistical classification approaches (Foody and Matur, 2006; Pal and Mather, 2004).
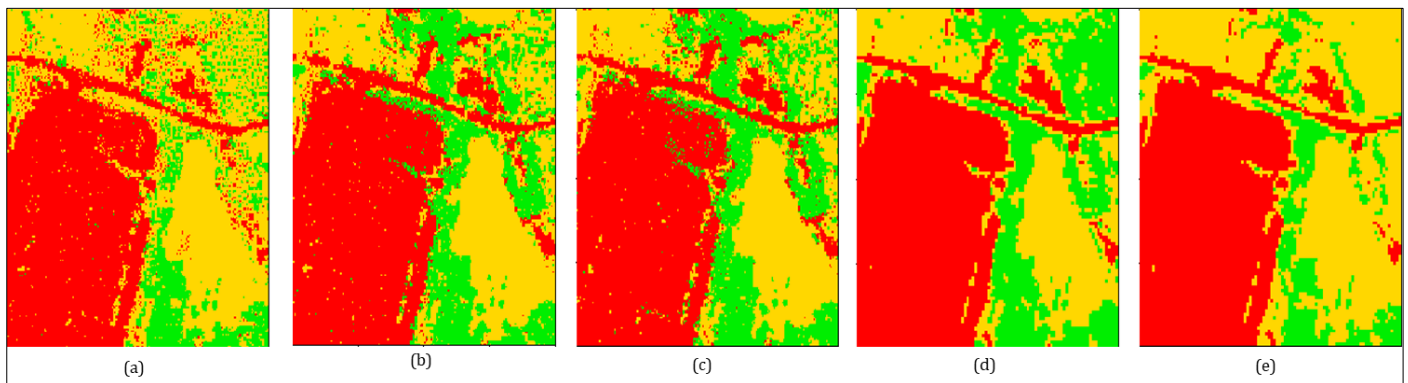
Fig. 5: (a), (b), (c) SRM generated at λ = 0.9 conventionally, SA and FCM techniques, (d) (e) SVM based and NN based reference images.

Table 6: Evaluation with SVM.

	Accuracy assessment with the SVM based reference data					
λ	SA based parameters		Conventional parameters		Fuzzy c-Means based parameters	
	OA	Kappa	OA	Kappa	OA	Kappa
0.9	83.34%	0.74	77.78%	0.67	83.67%	0.74
0.8	82.74%	0.73	77.75%	0.65	83.71%	0.74
0.7	81.26%	0.71	76.48%	0.64	82.40%	0.73

Table 7: Evaluation with NN.

	Accuracy assessment with the NN based reference data					
λ	SA based parameters		Conventional parameters		Fuzzy c-Means based parameters	
	OA	Kappa	OA	Kappa	OA	Kappa
0.9	81.70%	0.71	83.42%	0.72	82.39%	0.72
0.8	76.91%	0.64	79.35%	0.67	78.06%	0.66
0.7	75.63%	0.63	76.84%	0.63	76.67%	0.64

The NN was performed using a feed-forward NN classification technique, while SVM was implemented using radial basis function kernel on the resampled image of 1m resolution. Same training samples employed for the MLC has been used for both these classifications. This helps to keep the effect of the variation of size, composition and nature of the training data constant for all the classification techniques (Foody and Matur, 2006).

The SVM and NN classification-based reference images and the optimum SRM generated at a smoothness parameter of (λ) = 0.9 are shown in Fig. 5 below. The kappa statistics and the Overall Accuracy (OA) agreement between two SRM and the reference maps generated using SVM and the NN are shown in the Tables 6 and 7 separately.

For both the cases, the highest agreement between the reference images and the optimal SRM were achieved at λ = 0.9 as in the instance of MLC. For the SVM based comparison, the SA and FCM based SRM results shows a higher kappa agreement of 0.74 while for the conventional method, it is low as 0.67. In the case of NN based reference image, both the fuzzy and conventional based MRF models at λ= 0.9 show more of a similar result, with the average kappa agreement being 0.72. The poor inherent classification accuracy of the NN based reference image can have a significant effect on this result. The quality of the NN based classified image has shown a strong sensitivity to the training samples. As a condition of the study, we proposed to keep the training samples same for all the techniques we tested. Visual inspection shows a substantial confusion between the vegetation and the soil classes (Fig. 6(e)). Hence it is vital to use precise ground truth data in the case of NN to produce a more accurate validation dataset prior to the use of them as validation samples. The quantitative analysis and the visual inspection of overall results highlight the superiority achieved by the fuzzy class parameter definitions in the MRF models. These extended experiments also suggest the fitness for use of the proposed SRM model is consistent with respect to more familiar and frequently used parametric and non-parametric classification methods MLC, SVM and NN.

5   Summary

The work presented in this paper suggests an improved class parameter estimation using Fuzzy membership grades to determine the energy functions associated with conventional MRF. The inherent improvements followed by such an approach are summarized in detail. The fuzzy class parameters were defined using the SA and FCM techniques. The testing was done using a Worldview-II data set over a semi urban environment. The main assumptions made in the study were the selected training pixels to be pure elements of their representative land cover classes, the fine resolution pixels (y) are conditionally independent, fuzzy membership grade of a pixel (x) for a particular class is its proportion within that pixel and the observed pixel vector x_m of the multispectral image is having a Gaussian distribution with mean $\overline{\mu(x)}$ and covariance $\overline{\sum(x)}$ (equations (10) and (12)) defined using fuzzy definitions. The healthy class spectral seperability with TD and JM close

to 1.9 and 2.0 respectively suggested the least spectral confusion among the classes in the study area. This improves the selection of the pure spectral elements or the endmembers to define the reference pixel spectra for the SA based membership determination.

Minimization of the posterior energy for the optimum SRM c, (equation 15) was achieved using SA with Metropolis-Hasting sampler (Geman and Geman, 1984; Tso and Mather, 2009). The main parameter which controls the annealing schedule of SA technique is the initial temperature T_0 and the cooling schedule parameter (κ) which controls the rate of temperature decrease (Li 2009). Both these parameters are determined on the basis of the complexity of the problem at hand (Tolpekin and Stein, 2009). With the S = 2 and the higher class spectral seperability, the complexity of the classification problem addressed in this study is considerably low. For better results in complex situations, large values of both these parameters (T_0 = 3.0 and κ=0.9) which slows down the annealing process is recommended (Tolpekin and Stein, 2009). Regardless of the low complexity of the classification problem in this study, we have implemented a slow annealing process for better results as a precaution.

We test the fuzzy and conventional MRF models for a range of λ values from 0.3 to 0.9. Two different techniques, the spectral angle and the fuzzy c-means were used to define the fuzzy class parameters. This inclusion is mainly due to the difficulty in determining the best membership determination and to see the sensitivity of the models for such definitions. SRM generated for each of these λ parameters is a configuration of different spectral and contextual information combination. As a bench mark, these SRM results were comprehensively evaluated with respect to a standard parametric classification technique (MLC) at both pixel and sub pixel levels. In both the cases at a λ = 0.9 the optimum SRM were generated. The results demonstrate the significant improvements in the fuzzy MRF model, with smoother classification results. The FCM based fuzzy parameters produce slightly accurate images with respect to the SA based method for λ = 0.3 to 0.8. But very clearly both these methods produce the optimal SRM with a more of a same accuracy. This suggests that the sensitivity of the methods to varying fuzzy membership determinations can have little effect on the optimal result. But to strictly confirm this, extended work is needed. After carefully reviewing the MLC based results, experiments were drawn-out to compare the results with SVM and NN classifications.

The validation of the fuzzy MRF based SRM with the SVM based reference images has shown healthy classification agreement. The definition of the fuzzy mean and the covariance information for the classes has improved the spectral information modelled by the likelihood energy (equation 13) of the MRF model. The findings from using the NN classification have shown slightly different results. In this case, both the fuzzy and conventional MRF models have not been able to provide significantly different results, yet they did not deviate significantly on the basis of accuracy. Their agreement with the reference images are more of the same. As it has been pointed out earlier, the

generation of the reference data using NN to validate the MRF should be improved. The training samples used to determine the fuzzy and conventional mean and covariance parameters of the representative classes to model the PDF in the MRF is kept same for fuzzy as well as the conventional approaches. But it is understood that to improve the inherent classification accuracy of the NN based reference images it is better to use proper ground truth data, prior to the accuracy assessment. This kind of implementation can significantly change this result.

The overall results suggested that the proposed SA approach to generate fuzzy functional images is reasonable. It has produced results close in agreement with the well-known fuzzy c-means clustering membership grades. Using membership grades for the training pixels is observed to be advantageous as it also reduce the amount of representative training samples needed for the classification. The contextual information integration and the improvement of the class parameters using fuzzy definitions in the MRF based SRM technique, is proved to be more effective with better classification accuracy. For vague land cover interpretations, this approach can be very advantages due to its capabilities to reach higher classification accuracies at the sub pixel level. Further work is needed to test the performance of the method at a coarser resolution scale with heterogeneous land cover classes with strong similarity and also to validate the results with reference images having higher accuracy at sub pixel levels.

Fuzzy parameter integrated MRF based SRM technique employs an improved classification mechanism over the more reliable and frequently used classification methods such as MLC, SVM and NN. It is a classification technique which operates on a finer spatial resolution than that of the input image. As a relatively new field in Remote Sensing, different SRM techniques have shown the promise in determining thematic information using low resolution satellite data. Improving the technique to perform reliably in different applications is essential. In this work, certain efforts were taken to minimize the uncertainties that sneak into the SRM models due to the vague land cover interpretations, as well as the PSF using fuzzy definitions. The study went on to show that smoother and superior SRM maps were resulted with the use of fuzzy parameters.

Acknowledgement

Author Contributions

Conceptualization, methodology, analysis, writing—original draft preparation, D.R.W., and writing — review and editing, T.M.. All authors have read and agreed to the published version of the manuscript.

Conflict of Interest

The authors declare no conflict of interest.

References

Ardila, J., P., Tolpekin, V. A., Bijker, W., Stein, A., 2011. Markov-random-field-based super-resolution mapping for identification of urban trees in VHR images. ISPRS Journal of Photogrammetry and Remote Sensing. 66, 762-775.

Bastin, L., Fisher, P., Wood, J., 2002. Visualizing uncertainty in multi-spectral remotely sensed imagery. Computers & Geosciences. 28, 337-338.

Boardman, J. W., Inversion of imaging spectrometry data using singular value decomposition. Geoscience and Remote Sensing Symposium, 1989. IGARSS'89. 12th Canadian Symposium on Remote Sensing., 1989 International, Vol. 4, Vancouver, Canada 1989, pp. 2069-2072.

Canty, M. J., 2010. Image classification, and change detection in Remote Sensing with algorithms for ENVI/IDL. CRC Press, Boca Raton.

Congalton, R. G., 1991. A review of the assessing the accuracy of classification of Remotely Sensed data. Remote Sensing of Environment. 35-46.

DigitalGlobe. Vol. 2011, 2011.

Dubes, R. C., Jain, A. K., Nadabar, S. G., Chen, C. C., MRF Model-Based algorithm for image segmentation. 10th International Conference on Pattern Recognition, Vol. 1, Atlantic City, NJ, 1990, pp. 808 - 814

Duggin, M. J., Robinove, C. J., ,1990. Assumptions implicit in Remote Sensing data acquisition and analysis. International Journal of Remote Sensing. 11, 1169-1694.

Fisher, P., 1997. The pixel: a snare and a delusion. International Journal of Remote Sensing. 18, 679-685.

Fisher, P., 2010. Remote Sensing of land cover classes as type 2 fuzzy sets. Remote Sensing of Environment. 114, 309-321.

Fisher, P., Arnot, C., Wadsworth, R., Wellens, J., 2006. Detecting change in vague interpretations of landscapes. Ecological Informatics. 163-178.

Fisher, P. F., Pathirana, S., 1990. The evaluation of fuzzy membership of land cover classes in the suburban zone. Remote Sensing of Environment. 34, 121-132.

Foody , G. M., 1997. Fully fuzzy supervised classification of land cover from Remotely Sensed imagery with Artificial Neural Network. Neural Computing & Applications. 5, 238-247.

Foody, G. M., Matur, A., 2006. The use of small training sets containing mixed pixels for accurate hard image classification: Training on Mixed spectral

responses for classification by a SVM. Remote Sensing of Environment. 103, 179-189.

Forster, B., 1983. Some urban measurements from Landsat data. Photogrammetric Engineering and Remote Sensing. 49, 1693-1707.

Geman, S., Geman, D., 1984. Stochastic relaxation, Gibbs distribution, and the Bayesian restoration of images. IEEE Transactions on pattern analysis and machine intelligence. 6.

Kasetkasem, T., Arora, M. K., Varshney, P. K., 2005. Super-resolution land cover mapping using a Markov Random Field based approach. Remote Sensing of Environment. 96, 302-314.

Kasetkasem, T., Varshney, P. K., 2002. An Image change detection algorithm based on Markov Random field model. IEEE Transactions on Geoscience and Remote Sensing. 40, 1815-1823.

Krus, F. A., Lefkoff, A. B., Boardman, J. W., Heidebrecht, K. B., Shapiro, A. T., Barloon, P. J., Goetz, A. F. H., 1993. The Spectral image processing system (SIPS)-Interactive visualization and analysis of imaging spectrometer data. Remote Sensing of Environment. 44, 145-163.

Li, S. Z., 2009. Markov Random Field Modelling in image analysis. Springer-Verlag, London.

Maselli, F., Conese, C., Filippis, T. D., Norcini, S., 1995. Estimation of Forest Parameters Through Fuzzy Classification of TM Data. IEEE Transactions on Geoscience and Remote Sensing. 33, 77-84.

Pal, M., Mather, P. M., 2004. Assessment of the effectiveness of support vector machines for hyperspectral data. Future Generation Computer Systems. 20, 1215-1225.

Richards, J. A., Jia, X., 2006. Remote Sensing Digital Image Analysis. Springer-Verlag, Berlin Heidelberg.

Ridd, M. K., 1995. Exploring a V-I-S(Vegetation-impervious surface-soil) model for urban ecosystem analysis through remote sensing: comparative anatomy for cities. International Journal of Remote Sensing. 16, 2165-2185.

Sohn, Y., Moran, E., Gurri, F., 1999. Deforestation in North-Central Yucatan (1985-1995): Mapping secondary succession of forest and agricultural land use in sotuta using the cosine of the angle concept. Photogrammetric Engineering and Remote Sensing. 65, 947-958.

Solberg , A. H. S., Taxt, T., Jain, A. K., 1996. A Markov Random Field model for classification of multisource satellite imagery. IEEE Transactions on Geoscience and Remote Sensing. 34.

Tang, J., Wang, L., Myint, S. W., 2007. Improving urban classification through fuzzy supervised classification and spectral mixture analysis. International Journal of Remote Sensing. 28, 4047-4063.

Tolpekin, V. A., Stein, A., 2009. Quantification of the effects of land-cover-class spectral separability on the accuracy of Markov-Random-Field-Based Superresolution Mapping. IEEE Transactions on Geoscience and Remote Sensing. 47, 3283-3297.

Tso, B., Mather, P. M., 2009. Classification Methods for Remotely Sensed data. CRC Press, Boca Raton.

Wang, F., 1990. Fuzzy Supervised Classification of Remote Sensing Images. IEEE Transactions on Geoscience and Remote Sensing. 28, 194-201.

Welikanna, D. R, Tolpekin, V. A., Kant, Y., Analysis of the effectiveness of spectral mixture analysis and the Markov Random Field based Super Resolution Mapping over and Urban Environment. XXIst ISPRS Congress, Beijing, China, 2008, pp. 641-650.

Welikanna, D. R., Tamura, M., 2021. Lognormal Random Field models to identify temporal Land cover changes using full polarimetric L-Band SAR imagery. Journal of Geospatial Surveying, 1(1). DOI: https://doi.org/10.4038/jgs.v1i1.24.

Wood, T. F., Foody, G. M., 1993. Using cover-type likelihoods and typicalities in a geographic information system data structure to map gradually changing environments Landscape Ecology and GIS. 141-146.

Xu, M., Chen, H., Varshney, P. K., 2011. An image fusion approach based on Markov Random Fields. IEEE Transactions on Geoscience and Remote Sensing. 49, 5116-5127.

Zadeh, L. A., 1965. Fuzzy Sets. Information and Control. 8, 338-353.

Zhang, J., Foody, G. M., 2001. Fully-fuzzy supervised classification of sub-urban land cover from remotely sensed imagery: statistical and artificial neural network approach. International Journal of Remote Sensing. 22, 615-628.